Novel Magnetic-field-shifting Techniques in Asymmetric Rotor Pole Interior PM Machines with Enhanced Torque Density

Zi-Qiang Zhu, *Fellow*, *IEEE*, and Yang Xiao

Department of Electronic and Electrical Engineering, University of Sheffield, Sheffield S1 3JD, UK

This paper overviews novel magnetic-field-shifting techniques for enhancing the torque in a new class of asymmetric rotor pole interior permanent magnet (AIPM) machines. The principle for torque enhancement is introduced firstly. AIPM topologies are then categorized in terms of asymmetries and symmetricities of PM configuration and rotor core geometry. Subsequently, the merits and demerits of various AIPM rotor topologies in each category are analyzed and compared. Finally, torque capabilities of selected AIPM machines are compared.

***Index Terms*—Asymmetric interior permanent magnet (AIPM), Magnetic-field-shifting (MFS), PM torque, Reluctance torque**

I. Introduction

PERMANENT magnet (PM) machines have been rapidly developed in recent decades after invention and application of PM materials with high energy product, including high remanence and coercivity, such as SmCo and NdFeB [1]-[3]. According to the position of PMs in the rotor core, PM machines can be generally classified as surface-mounted PM (SPM) machines and interior PM (IPM) machines with PMs placed on the surface of rotor core and buried inside the rotor core, respectively [4]. In recent years, IPM machines are of growing interests in many applications including electric vehicles (EVs) [5]-[8], electric aircrafts and helicopters [9]-[10], marine propulsions [11], and aerospace applications [12] due to superior torque density, high efficiency, wide constant power operation speed range (CPSR), and high rotor robustness. Besides, IPM machines can utilize the reluctance torque resulted from the rotor saliency to enhance the torque density without introducing additional PM usage [13].

In literature, many conventional rotor topologies of IPM machines have been documented, such as Bar-shape [14], V-shape [14]-[16], Delta-shape [16], double-V shape [17], spoke-type [18] rotor structures. Besides, multi-layer rotor topologies that are often designated as PM assisted synchronous reluctance machines have also been widely studied [19]-[20]. However, in these conventional IPM machines with symmetrical rotor structures, maximum PM and reluctance torque components are reached at different current angles whose difference is theoretically 45 electrical degrees. Consequently, only a portion of both torque components can be utilized for maximum synthetic torque. To deal with this issue, asymmetric rotor pole IPM (AIPM) rotor topologies are introduced to utilize a novel design concept designated as magnetic-field-shifting (MFS) effect for torque enhancement in IPM machines by making the current angles for maximum PM and reluctance torque components closer.

This paper overviews the MFS techniques in various novel AIPM rotor topologies. The principle for torque enhancement by utilizing MFS effect in AIPM machines is introduced in Section II. Various AIPM machine topologies are categorized by the proposed categorization method in terms of asymmetries and symmetricities of PM configurations and rotor core geometries, while the merits and demerits of AIPM machines in each category are analyzed and compared in Section III. In Section IV, several selected AIPM machines are redesigned based on the conventional IPM machine benchmark for Toyota Prius 2010 and their performance are compared. Besides, experimental results of an AIPM machine prototype are provided for verification. Section V is the conclusion.

II. Principle for Torque Enhancement

In this section, the principle of utilizing MFS effect in AIPM machines to enhance torque density is introduced by a simplified analytical model that ignores saturation, cross-magnetization and harmonics.

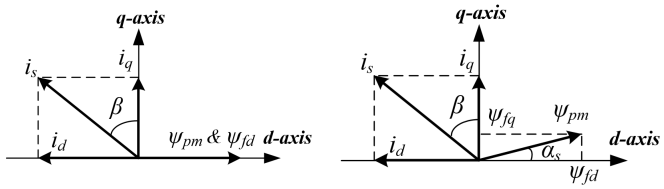

(a) (b)

Fig. 1. Vector diagrams in *d*-*q* axis coordinates. (a) Conventional IPM machine. (b) AIPM machine.

The vector diagrams of stator current and PM flux linkage in conventional IPM and AIPM machines are shown in Fig. 1, where i_s, i_d, and i_q are the vectors of stator current and *d*- and *q*-axis currents, respectively; ψ_{pm}, ψ_{fd}, and ψ_{fq} are the vectors of synthetic PM flux linkage and *d*- and *q*-axis PM flux linkages, respectively, β is the current advancing angle, and α_s is the asymmetric angle in AIPM machine. The *d*-*q* axis coordinates in Fig. 1 are defined by the rotor saliency.

The *d*- and *q*-axis flux linkages can be generally expressed as (1), where ψ_d and ψ_q are the *d*- and *q*-axis flux linkages, L_d and L_q are the *d*- and *q*-axis inductances.

$$\begin{cases} \psi_d = \psi_{fd} + L_d i_d \\ \psi_q = \psi_{fq} + L_q i_d \end{cases} \tag{1}$$

According to Fig. 1 and (1), the *d*- and *q*-axis flux linkages in IPM and AIPM machines are expressed as (2) and (3), respectively,

This article has been accepted for publication in a future issue of this journal, but has not been fully edited. Content may change prior to final publication. Citation information: DOI 10.1109/TMAG.2021.3076418, IEEE Transactions on Magnetics

$$\begin{cases}\psi_d = \psi_{pm} - L_d i_s \sin\beta \\ \psi_q = L_q i_s \cos\beta \end{cases} \tag{2}$$

$$\begin{cases}\psi_d = \psi_{pm} \cos\alpha_s - L_d i_s \sin\beta \\ \psi_q = \psi_{pm} \sin\alpha_s + L_q i_s \cos\beta \end{cases} \tag{3}$$

The general torque equations for IPM machines are shown in (4), which includes the PM torque component produced by the interaction between q-axis PM flux linkage ψ_{fq} and d-axis current i_d for AIPM machines.

$$\begin{cases} T_e = T_m + T_r \\ T_m = \dfrac{3p}{2}(\psi_{fd} i_q + \psi_{fq} i_d) \\ T_r = \dfrac{3p}{2}(L_d - L_q) i_d i_q \end{cases} \tag{4}$$

where T_e, T_m, and T_r are the synthetic, PM, and reluctance torque components, respectively, p is the number of pole pairs.

Therefore,

$$\begin{cases} T_m = \dfrac{3p}{2}\psi_{pm} i_s \cos\beta \\ T_r = \dfrac{3p}{4}(L_q - L_d) i_s^2 \sin 2\beta \end{cases} \tag{5}$$

for conventional IPM machines, and

$$\begin{cases} T_m = \dfrac{3p}{2}\psi_{pm} i_s \cos(\beta - \alpha_s) \\ T_r = \dfrac{3p}{4}(L_q - L_d) i_s^2 \sin 2\beta \end{cases} \tag{6}$$

for AIPM machines.

Thus, the synthetic torques of conventional IPM and AIPM machines can be expressed as

$$\begin{cases} T_{e-IPM} = T_{pm} \cos\beta + T_{rel} \sin 2\beta \\ T_{e-AIPM} = T_{pm} \cos(\beta - \alpha_s) + T_{rel} \sin 2\beta \end{cases} \tag{7}$$

where

$$\begin{cases} T_{pm} = \dfrac{3p}{2}\psi_{pm} i_s \\ T_{rel} = \dfrac{3p}{4}(L_q - L_d) i_s^2 \end{cases} \tag{8}$$

The torque-angle performances of IPM and AIPM machines are compared in Fig. 2, where T_{syn}, T_{pm} and T_{rel} are the amplitudes of synthetic, PM and reluctance torque components, respectively, $\triangle\beta$ is the current angle difference between the maximum points of PM and reluctance torque components.

As shown in (7), the PM and reluctance torque components in conventional IPM machines reach the maximum points when β are 0 and 45 electrical degrees (ED), respectively, while the peak points of PM and reluctance torque components in AIPM machines are reached when β are α_s and 45 ED, respectively. Consequently, the current angle difference in conventional IPM machines is theoretically $\triangle\beta$ = 45 ED, while the maximum points of PM and reluctance torques in AIPM machines are shifted to be closer and becomes $\triangle\beta$ = 45-α_s ED with a positive α_s due to the MFS effect, as shown in Fig. 2. Thus, synthetic torque is enhanced without the increase of both PM and reluctance torque amplitudes in AIPM machines compared with IPM machines.

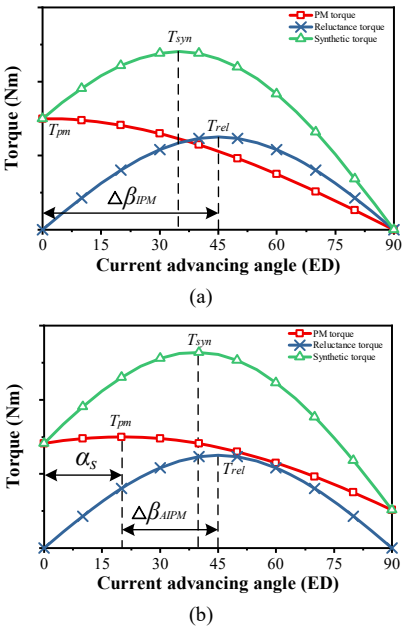

Fig. 2. Torque-current angle characteristics. (a) Conventional IPM machine. (b) AIPM machine.

III. Techniques for Torque Enhancement in AIPM Machine Topologies

The concept of MFS effect for torque enhancement in novel AIPM machine was firstly proposed by setting the optimal displacement angle between the SPM rotor and the reluctance rotor in a hybrid rotor asymmetric PM machine with two rotor parts [21] and by employing asymmetric rotor flux barriers in an IPM machine with symmetrical V-shape PMs [22], respectively. Subsequently, numerous different AIPM rotor topologies have been developed. In this section, a categorization method for AIPM rotor topologies are proposed and various topologies in each category are presented and analyzed.

TABLE I
Categories of AIPM Machine Topologies

Category	PM configuration	Rotor core geometry
Group I	Symmetrical	Symmetrical
Group II	Symmetrical	Asymmetric
Group III	Asymmetric	Symmetrical
Group IV	Asymmetric	Asymmetric

A. Categorization Method for AIPM Topologies

In conventional IPM machines, both PM configuration and rotor core geometry are symmetrical. In order to utilize the MFS effect for torque density enhancement, AIPM rotor topologies are required in IPM synchronous machines. There are many techniques for realizing the MFS. To ease the discussions of various AIPM topologies with different rotor structures, a categorization method is proposed according to whether PM configuration and rotor core geometry are symmetrical or asymmetrical, respectively. Thus, as shown in Table I and Fig. 3, in total there are four groups based on the proposed categorization method. In Fig. 3, PMs in red and

This article has been accepted for publication in a future issue of this journal, but has not been fully edited. Content may change prior to final publication. Citation information: DOI 10.1109/TMAG.2021.3076418, IEEE Transactions on Magnetics

blue denote N- and S-poles, respectively.

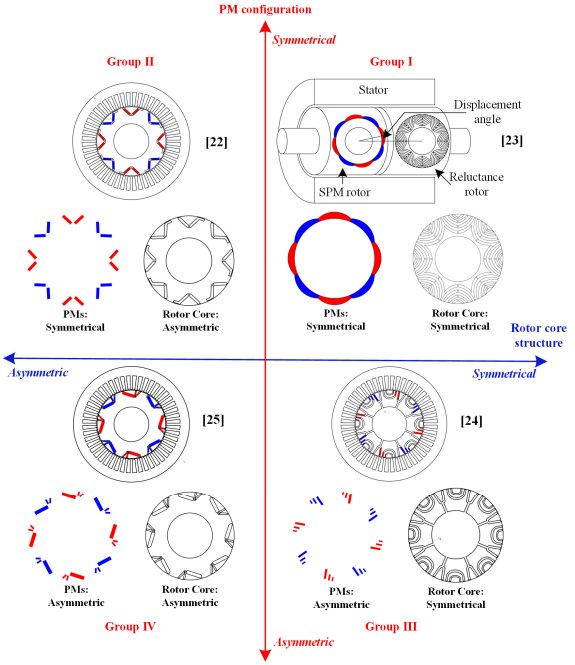

Fig. 3. Categorization method of AIPM machine topologies.

In an AIPM machine with two-part rotor [23], both PM configuration in the SPM rotor part and geometry of the multi-layer reluctance rotor part are symmetrical, Group I, and MFS effect is utilized by adjusting the displacement angle between two rotor parts. The AIPM machine in [22] has symmetrical V-shape PMs but the rotor geometry is asymmetric due to additional flux barrier at right side of PMs in each pole, Group II. [24] proposes a multi-layer AIPM machine topology with symmetrical flux barrier structure but asymmetric PMs, Group III. A hybrid-layer AIPM machine topology, namely one part of the PM configuration in each pole has one layer while the other part has two layers, is proposed in [25] that has both asymmetric PMs and rotor core structures, Group IV. Based on the proposed method, the AIPM machine topologies can be categorized and overviewed based on their associated categories in this section.

B. Group I - Symmetrical PMs and Symmetrical Rotor Core

Hybrid rotor PM machines combining the SPM rotor part and the synchronous reluctance rotor part using axially laminated anisotropic (ALA) structure have been proposed to improve the flux weakening capability and achieve wide CPSR in literature [26]-[29] for EV applications, as shown in Fig. 4. The reported hybrid PM rotor machine that uses longer axial length of SPM rotor part (L2) than that of ALA rotor part (L1) shows wider CPSR than SPM machine and higher efficiency than induction machines.

As the initial studies [26]-[29] ignore the adjustment of displacement angle between two rotor parts while only use rotor designs in which PM axis in SPM part and rotor saliency axis of ALA part are aligned. The displacement angle γ between SPM and reluctance rotor parts is introduced in [27], but only two cases where *d*-axis of SPM rotor part is aligned with *d*-axis (γ=0 ED) and *q*-axis (γ=90 ED) of reluctance rotor part, respectively, are considered. [30] investigates the effect of displacement angle between two rotor parts in a two-part hybrid rotor PM machine with IPM and circular ALA parts as shown in Fig. 5. It is found that torque enhancement can be achieved with appropriate displacement angle γ in the hybrid rotor asymmetric PM (HRAPM) machine. Later, HRAPM machine has been theoretically analyzed in [21], which reveals that the torque enhancement is due to utilizing MFS effect.

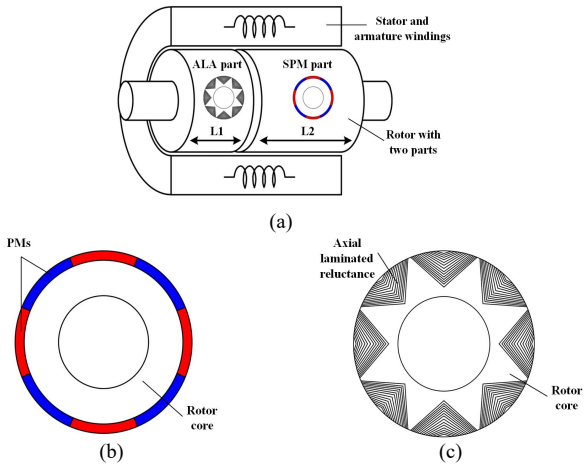

Fig. 4. Hybrid PM rotor machine with two rotor parts [26]-[29]. (a) Machine topology. (b) SPM rotor part. (c) Reluctance rotor part with ALA structure.

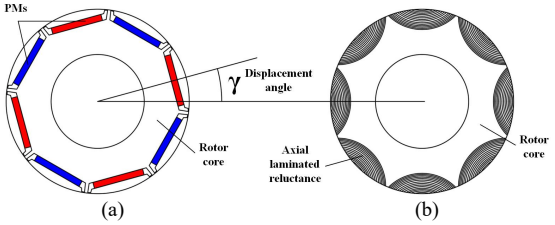

Fig. 5. Hybrid PM rotor machine with displacement angle between two rotor parts [30]. (a) IPM rotor part. (c) Reluctance rotor part with ALA structure.

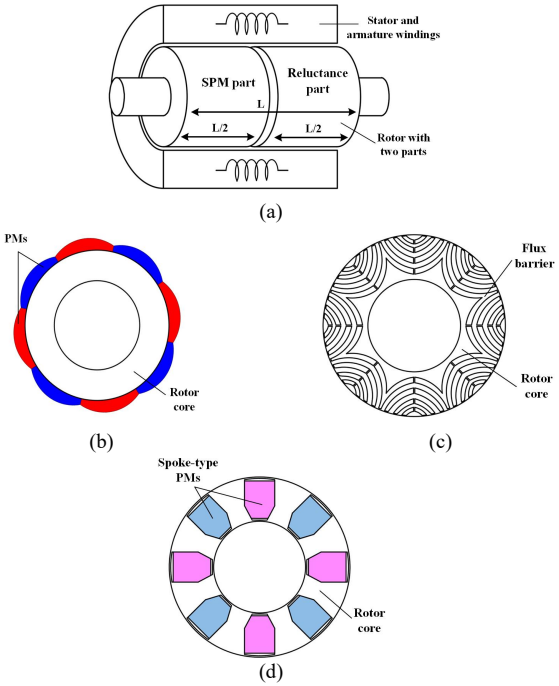

Fig. 6. HRAPM machine with two-part rotor. (a) Machine topology [23], [31]-[32]. (b) SPM rotor part with shaped PMs [23]. (c) Multi-layer reluctance rotor part [23]. (d) Spoke-type IPM rotor part with ferrite PMs [32].

This article has been accepted for publication in a future issue of this journal, but has not been fully edited. Content may change prior to final publication. Citation information: DOI 10.1109/TMAG.2021.3076418, IEEE Transactions on Magnetics

Two-part rotor HRAPM machines are shown in Fig. 6 (a) in which SPM and reluctance rotor parts have the same axial length. In [23] and [31], HRAPM machines with SPM and multi-layer reluctance rotor parts are used and the maximum PM and reluctance torque components can be achieved at approximately the same current advancing angle. Shaped PMs shown in Fig. 6 (b) are employed in [23] to reduce the torque ripple. Moreover, IPM rotor with non-rare earth PMs can also be a candidate for the reluctance rotor part, as [32] uses the spoke-type IPM rotor with ferrite PMs shown in Fig. 6 (d) to improve efficiency and to reduce expensive rare-earth PM usage.

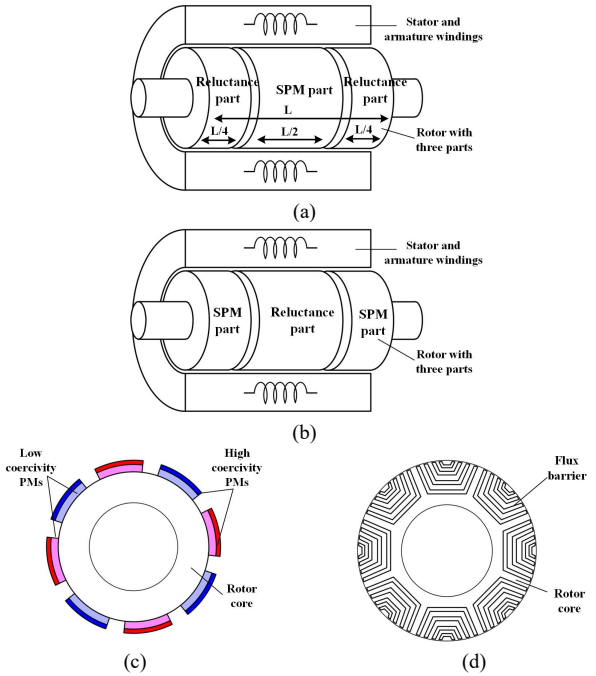

Fig. 7. HRAPM machine with three-part rotor. (a) Machine topology with two reluctance rotor parts [33]. (b) Machine topology with two SPM rotor parts [34]. (c) SPM rotor with hybrid PMs [35]. (d) Four-layer reluctance rotor [35].

To mitigate the issue of unbalanced axial electromagnetic force in two rotor parts HRAPM machine [33], rotor structure with three parts that uses the same rotor parts at both axial ends is proposed [33]-[35] as shown in Fig. 7, while the displacement angle between both rotor end parts and the central part is optimized to better utilize the MFS effect. The topology with the SPM rotor sandwiched by two multi-layer reluctance rotors is proposed in [33] that has higher average torque and lower torque ripple than a PM-assisted synchronous reluctance machine. [34] presents a three-part rotor HRAPM machine with the reluctance rotor sandwiched by two SPM rotor parts. To further extend the CPSR, variable PM material magnetization state concept is implemented in the three rotor parts HRAPM machine in [35] that uses a SPM rotor with hybrid PMs connected in series shown in Fig. 7 (c) and a four-layer reluctance rotor shown in Fig. 7 (d). By adjusting magnetization states of low coercivity PMs, CPSR extension can be achieved.

Overall, asymmetric multiple rotor part PM machines discussed in Figs. 5-7 have symmetrical PM configurations and rotor core geometries and can be generally perceived as an axial hybridization of SPM or IPM machines and synchronous reluctance machines. MFS effect is utilized by adjusting displacement angle between PM and reluctance rotor parts. Therefore, the topologies of rotor parts can be simple and the maximum points of PM and reluctance torque components can be easily aligned. However, the assembly of rotor parts makes HRAPM machines mechanically complicated. Moreover, as only part of the stator is utilized for PM magnetic flux, the back electromotive (EMF) and PM torque components are restricted due to stator core saturation.

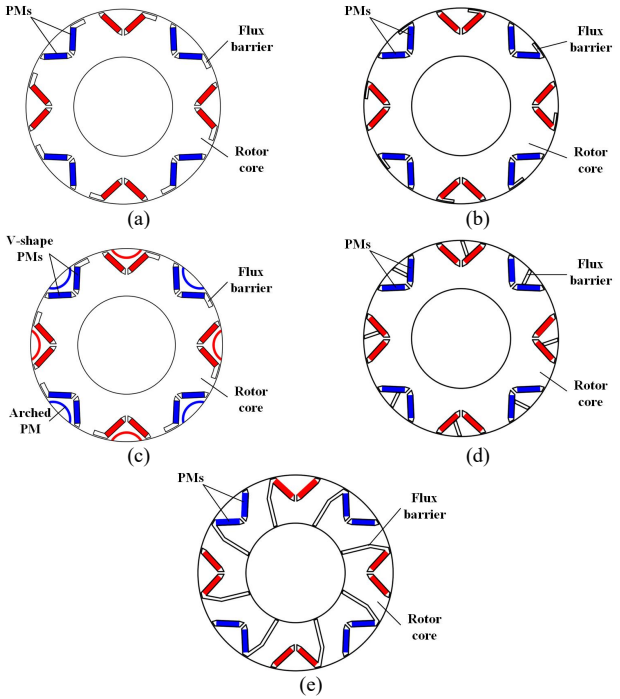

Fig. 8. AIPM rotor topologies with symmetrical V-shape PMs and asymmetric rotor core. (a) Flux barriers near rotor surface and outside PMs [21]. (b) Flux barriers near rotor surface and inside PMs [36]. (c) Extra arc PMs and flux barriers outside PMs [37]. (d) Flux barriers inside PMs and between rotor surface and PMs [38]-[39]. (e) Asymmetric spoke-type flux barriers [40].

C. Group II - Symmetrical PMs and Asymmetric Rotor Core

To deal with the issues of multiple rotor parts in HRAPM machines, the AIPM rotor topology using only one rotor with conventional symmetrical PM configuration and asymmetric rotor core geometry, i.e. employing asymmetric flux barriers to utilize MFS effect, is proposed firstly in [21]. The AIPM machine topology has symmetrical V-shape PMs and asymmetric flux barriers outside the V-shape PM cavity that is located at the right-side PM near the rotor surface in each pole as shown in Fig. 8 (a), which utilizes MFS effect by shifting the position of reluctance axes. An AIPM machine rotor topology is proposed in [36] as shown in Fig. 8 (b), but the flux barrier is located inside the V-shape PMs. Both novel AIPM machines can achieve obvious torque enhancement. Besides, it is found that the flux barrier design in Fig. 8 (b) influences both PM and reluctance torque components but flux barriers in Fig. 8 (a) show negligible effects on PM field and PM torque. [37] employs additional arc PM and asymmetric flux barriers near the right side of V-shape PMs in each pole based on [21] as shown in Fig. 8 (c). The proposed

This article has been accepted for publication in a future issue of this journal, but has not been fully edited. Content may change prior to final publication. Citation information: DOI 10.1109/TMAG.2021.3076418, IEEE Transactions on Magnetics

machine shows significant torque enhancement and torque ripple reduction simultaneously compared with the Toyota Prius 2004. However, more PMs are used and the thin arc PM causes concerns for potential demagnetization.

Different from flux barriers near the rotor surface in [21] and [36]-[37], an AIPM machine rotor topology with V-shape PMs is proposed in [38] and analyzed in [39], which employs a flux barrier inside the PM cavity in each pole while the outer and inner ends are located near the rotor surface and near a PM, respectively, as shown in Fig. 8 (d). The comparison indicates that small torque enhancement and torque ripple reduction can be achieved by the proposed machine due to diminishing negative torque components resulted from cross magnetization effect. However, as fractional slot concentrated windings are employed in the studied machine [39], the MFS is insignificant because of small reluctance torque. Asymmetric spoke-type flux barriers whose outer and inner ends are located near the outer and inner surfaces of the rotor are employed in a V-shape AIPM machine [40], as shown in Fig. 8 (e). In this novel design, the increase of torque density can be achieved compared with the conventional V-shape IPM with the same total volume of PMs, although the improvement is not significant. However, this topology raises mechanical issue due to flux barrier structure.

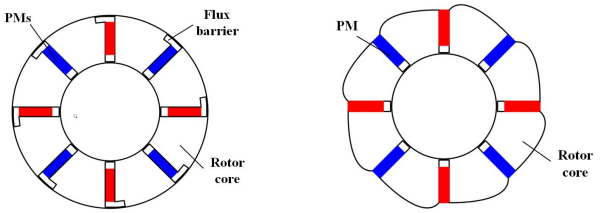

Fig. 9. AIPM machine rotor topologies with symmetrical spoke-type PMs and asymmetric rotor core. (a) Asymmetric flux barrier [41]. (b) Asymmetric rotor profile [42].

Asymmetric rotor geometry can also be used in spoke-type AIPM machine rotor topologies. Extra asymmetric flux barriers near rotor surface are employed in [41] as shown Fig. 9 (a), which can utilize both flux-focusing and MFS effects to enhance torque density while notably reduce cogging torque simultaneously. Asymmetric rotor profile is applied in a spoke-type AIPM machine [42] (Fig. 9 (b)) to reduce magnetic field harmonics introduced by PM magnetic flux density, thereby significantly reducing both torque ripple and vibration albeit with small decrease of average torque.

In summary, the AIPM machine rotor topologies discussed in Figs. 8 and 9 generally employ additional asymmetric flux barriers in conventional IPM machines to utilize MFS effect by shifting the axis of rotor saliency. Thus, rotor structures are generally simple for easy manufacturability. However, the enhancement of torque density is generally relatively small and flux barrier designs especially for topologies with thin ribs may raise mechanical stress issues.

D. Group III - Asymmetric PMs and Symmetrical Rotor Core

Except for employing asymmetric rotor core to shift the reluctance axis, MFS effect can also be utilized by using asymmetric PM configuration as it can adjust the relative position between PM field and reluctance axes. Various AIPM machine rotor topologies with asymmetric PMs and symmetrical rotor cores have been proposed in literature.

The AIPM machine rotor topology with asymmetric PM configuration was firstly introduced by using inset PMs in [43], Fig. 10 (a), as the axis of PM field can be easily shifted by asymmetric PM position. Compared with an SPM machine, the AIPM machine with shifted inset PM position in [43]-[45] shows increased torque density, improved CPSR, and reduced losses. A similar topology with hybrid pole configurations, i.e. adjacent poles using asymmetric inset PMs and symmetrical V-shape PMs alternatively, has been proposed and employed in an IPM machine in [46] and [47] as shown in Fig. 10 (b). The hybrid pole AIPM machine shows torque enhancement and torque ripple reduction compared with a V-shape IPM benchmark, although the torque density is slightly smaller than the symmetrical inset IPM benchmark. Besides, compared with IPM machines whose PMs are buried inside the rotor core, the AIPM machine with inset PMs may require mechanical retaining such as rotor sleeve for high speed operation.

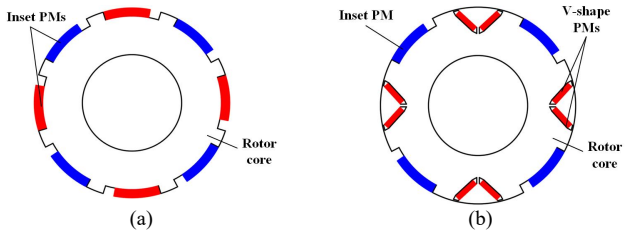

Fig. 10. AIPM machine rotor topologies with asymmetric inset PMs and symmetrical rotor core. (a) Asymmetric inset PMs [43]-[45]. (b) Hybrid pole topology with asymmetric inset PMs and symmetrical V-shape PMs [46]-[47].

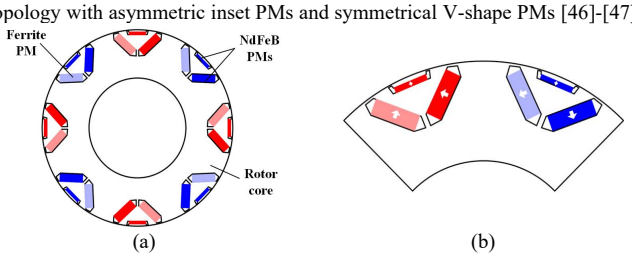

Fig. 11. AIPM machine rotor topology with hybrid PMs and symmetrical Delta-shape rotor core [48]. (a) Rotor topology. (b) Magnetization directions of PMs

Hybrid PM configuration combining NdFeB and ferrite PMs is also employed [48] as shown in Fig. 11 in a Delta-shape AIPM machine, while the direction in PMs denotes the magnetization direction as illustrated in Fig. 11 (b). Compared with a double-bar shape IPM machine for BMW i3 with the same NdFeB PM usage, the increase of maximum torque and power can be achieved across the whole speed range with torque ripple reduction. MFS effect is obvious from the performance improvement of torque components versus current angles. However, due to higher amplitudes of magnetic field harmonics, the AIPM machine has lower efficiency at high speed.

In various multi-layer AIPM machine topologies [49]-[52], asymmetric PM configurations and symmetrical multi-layer rotor geometries are applied to utilize MFS effect while maintaining the merit of high reluctance torque in PM assisted synchronous reluctance machines, as shown in Fig. 12. [49]

This article has been accepted for publication in a future issue of this journal, but has not been fully edited. Content may change prior to final publication. Citation information: DOI 10.1109/TMAG.2021.3076418, IEEE Transactions on Magnetics

proposes a multi-layer AIPM topology with inset PMs in *q*-axis near the rotor surface, as shown in Figs. 12 (a) and (b). The AIPM machine shows higher average torque and smaller torque ripple compared with a symmetrical multi-layer IPM machine with similar structure. Besides, the efficiency of AIPM machine across the investigated speed range has been improved due to torque enhancement and iron loss reduction. A novel AIPM machine with spoke-type flux barrier in *q*-axis [24] is shown in Figs. 12 (c) and (d), which shows torque enhancement compared with a conventional three-layer PM assisted reluctance machine with circular cavities due to fully aligned maximum PM and reluctance torque components. The increase of torque and reduction of torque ripple also clearly exist in an AIPM machine with three-layer structure [50] and an AIPM machine with spoke-type PMs in *d*-axis between the second and fourth layers [51], compared with their conventional PM-assisted reluctance machine benchmarks, respectively.

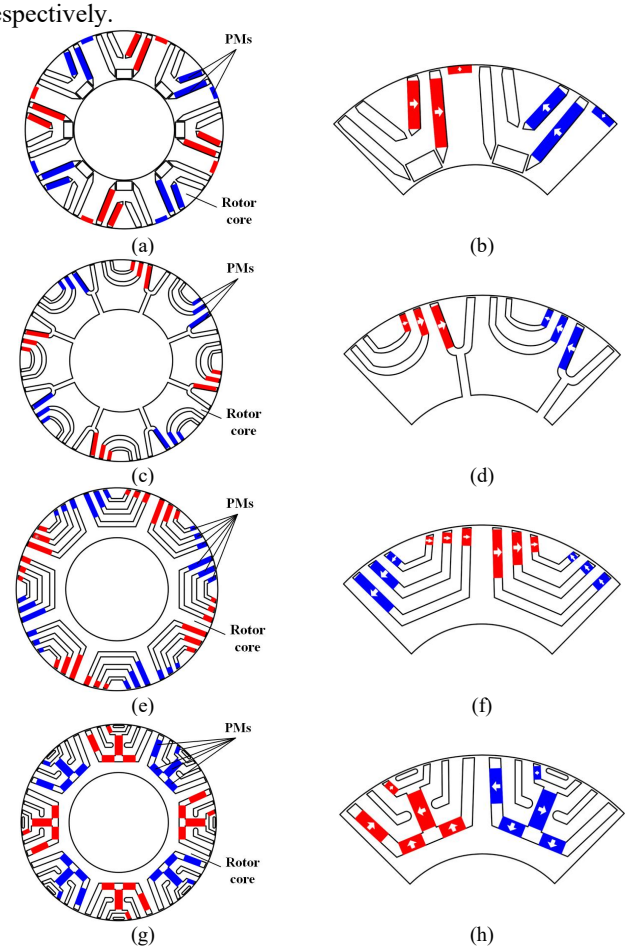

Fig. 12. AIPM machine rotor topologies with symmetrical multi-layer rotor geometries. (a) Rotor topology with inset PMs in *q*-axis [49]. (b) PM magnetization directions of (a). (c) Rotor topology with *q*-axis spoke-type flux barrier [24]. (d) PM magnetization directions of (c). (e) Rotor topology with three-layer geometry [50]. (f) PM magnetization directions of (e). (g) Rotor topology with spoke-type PMs in *d*-axis [51]. (h) PM magnetization directions of (g).

However, for these AIPM machines with multi-layer structures, the PM usage is restricted in the AIPM machine topology as only part of the PM cavity is available for burying PMs. Besides, even compared with conventional multi-layer IPM machines, AIPM machines show complicated geometry and multiple PMs with different dimensions, which makes the manufacturing and assembling complex.

In summary, three approaches to develop AIPM machine topologies with asymmetric PMs and symmetrical rotor core structures for utilizing MFS effect are reported in literature. By employing asymmetric inset PMs, AIPM machines can be achieved using simple structures and are shown clear torque enhancement, but the CPSR performance has not been investigated in references. The AIPM machine employing hybrid PMs has enhanced torque density without the increase of rare-earth PM usage by using simple mechanical structure. Multi-layer AIPM topologies can achieve significant increase of average torque, but the topologies are complex due to many pieces of PMs with different dimensions and complicated rotor core geometry.

E. Group IV - Asymmetric PMs and Asymmetric Rotor Core

As illustrated in the previous sections, either asymmetric PM configuration or asymmetric rotor core geometry can adjust the axes of PM field and reluctance torque components, respectively. By employing both asymmetric PMs and rotor core the MFS effect in AIPM machines can be better utilized for torque enhancement with more freedoms of design. Various novel AIPM machine topologies with asymmetric PMs and asymmetric rotor core geometry are proposed in recent years, as overviewed below.

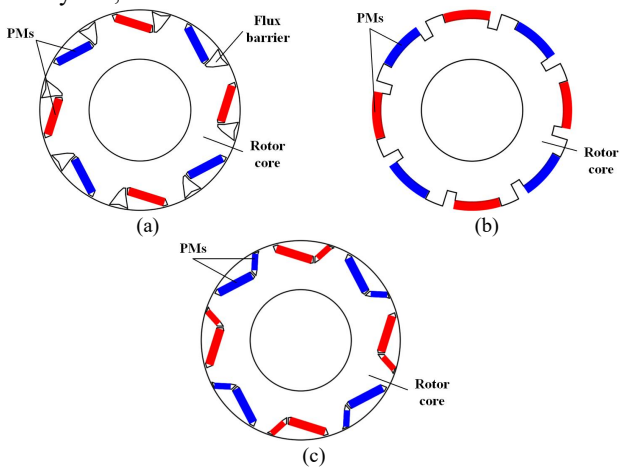

Fig. 13. AIPM machine rotor topologies with asymmetric single-layer PMs and rotor cores. (a) Asymmetric bar-shape AIPM machine [36], [52]-[53]. (b) AIPM machine with inset PMs [54]. (c) AIPM machine with asymmetric V-shape PMs [55].

Several AIPM machines with single layer asymmetric PMs and asymmetric rotor core are shown in Fig. 13. An AIPM machine rotor topology with asymmetric bar-shape PMs and extra flux barrier in each pole whose outer and inner ends are located near the rotor surface and right side of the PM in each pole, respectively, has been proposed and analyzed in [36], [52] and [53], as shown in Fig. 13 (a). Compared with the conventional bar-shape IPM machine benchmark, significant enhancement of torque density per magnet volume can be achieved. The AIPM machine with asymmetric inset PMs [54] as shown in Fig. 13 (b) shows the increase of torque compared with a conventional SPM machine due to fully aligned maximum PM and reluctance torque components. An AIPM machine exhibiting single layer asymmetric V-shape PMs

This article has been accepted for publication in a future issue of this journal, but has not been fully edited. Content may change prior to final publication. Citation information: DOI 10.1109/TMAG.2021.3076418, IEEE Transactions on Magnetics

with different PM dimensions is proposed in [55], which has negligible increase of average torque since MFS effect can hardly be utilized.

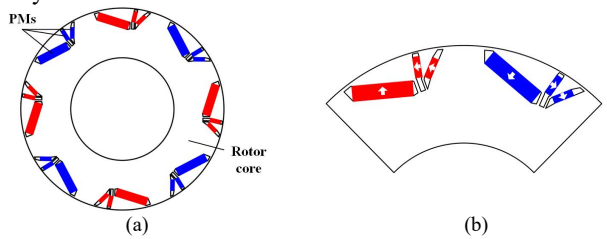

Fig. 14. AIPM machine rotor topology with hybrid-layer PMs [25]. (a) Rotor topology. (b) PM magnetization directions.

[25] proposes a hybrid-layer AIPM machine rotor topology, i.e. a part of the PM configuration in each pole has single-layer PM and the other part has double-layer PMs, as shown in Fig. 14, or in general, different numbers of layers at two sides of each pole. Compared with the conventional V-shape IPM machine using the same volume of PMs, significant torque enhancement, torque ripple reduction, and CPSR extension can be achieved simultaneously. Similar demagnetization withstand capability to the V-shape IPM benchmark is also proved for the proposed AIPM machine, with slightly complicated rib structures.

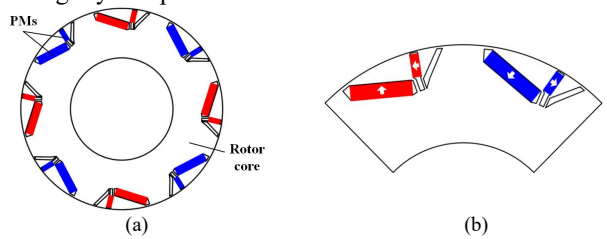

Fig. 15. AIPM machine rotor topology with asymmetric V-shape PMs and outside flux barrier [56]. (a) Rotor topology. (b) PM magnetization directions.

In [56], an AIPM rotor topology with asymmetric V-shape PMs and extra flux barriers outside the PMs is proposed for IPM synchronous machines as shown in Fig. 15. The outer and inner ends of flux barrier are located near the rotor surface between adjacent V-shape PMs and near the bottom of asymmetric PM cavity, respectively. The proposed AIPM machine with outer flux barrier [56], Fig.15, and the AIPM machine with inner flux barrier [38]-[39], Fig. 8(d), are designed with the same stator, rotor diameter and PM usage to the conventional V-shape IPM machine for Toyota Prius 2010 and final optimal machines are compared. It confirms the proposed AIPM machine with outer flux barriers shows inherently higher torque density than the AIPM machine with inner flux barrier structure, as will be further described in Section IV.B. Compared with the IPM machine benchmark, significant torque enhancement is achieved by employing the proposed AIPM topology. Besides, the improved CPSR, efficiency and thermal performances in the AIPM machine with outer flux barriers are also revealed.

Mixed radial and circumferential AIPM machine rotor topologies are proposed in [57] and [58], where the spoke-type PM is regarded as a half layer because its magnetomotive force (MMF) and magnetic reluctance are shared by magnetic circuits of adjacent poles, as shown in Fig. 16. [57] uses spoke-type PMs and shifted bar-shape PMs that shows significant improvement of torque capability and demagnetization withstand capability compared with the similar symmetrical design. In [58], the AIPM machine topology employs spoke-type PMs, shifted V-shape PMs and additional asymmetric flux barriers. Compared with a V-shape IPM machine benchmark, the novel mixed radial and circumferential AIPM machine has significant enhancement of torque density and improvement of CPSR performance by using the same stator, rotor diameter and total PM usage. Besides, the mechanical analysis shows no concern of von-Mises stress.

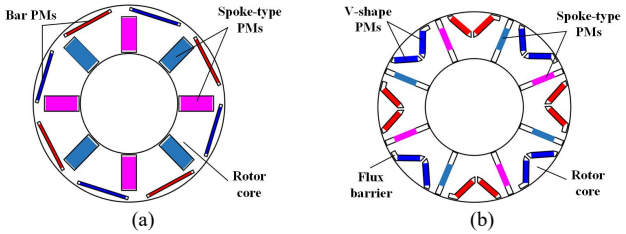

Fig. 16. Mixed radial and circumferential AIPM machine rotor topologies. (a) AIPM machine with bar-shape and spoke-type PMs [57]. (b) AIPM machine with V-shape and spoke-type PMs and additional flux barrier [58].

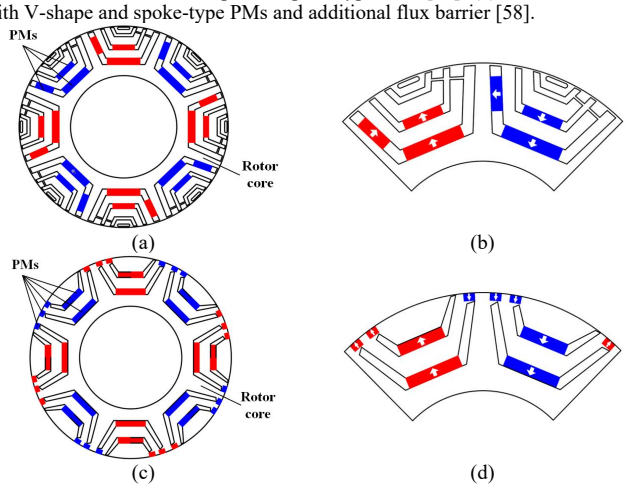

Fig. 17. Multi-layer AIPM machine rotor topologies with asymmetric PMs and rotor core. (a) AIPM machine with four-layer reluctance and two-layer asymmetric PMs [51]. (b) AIPM machine with multiple asymmetric inset PMs [59].

Several multi-layer AIPM machine topologies with asymmetric PMs and rotor cores are also proposed in [51] and [59], as shown in Fig. 17. Torque enhancement due to utilizing MFS effect has been found in both machines, although no further performance investigation has been reported. However, these topologies are very complicated because of multi-layer rotor core, complex slot and rib structure, and multiple PMs with different dimensions.

In conclusion, AIPM machine topologies with both asymmetric PMs and rotor core geometries provide more freedoms of design and many associated novel designs have been proposed. Some AIPM machines in this category with relatively simple structures have significant torque enhancement due to notable MFS effect and improvements of other performance including torque ripple, efficiency and CPSR, compared with conventional IPM benchmarks.

IV. Comparison of Selected AIPM Machines

A. Comparison between AIPM Machines and Toyota Prius 2010 IPM Machine

To illustrate the MFS effect for torque density enhancement in various AIPM machine topologies, six typical AIPM rotor topologies in four categories, including AIPM-SS [23] in Figs. 6 (a)-(c), AIPM-SA [22] in Fig. 8 (a), AIPM-AS [46]-[47] in Fig. 10 (b), as well as AIPM-AA1 [25], AIPM-AA2 [56], and AIPM-AA3 [57] that are shown in Figs. 14-15 and Fig. 16 (b) respectively, are redesigned with the same stator, rotor diameter, and PM usage to the conventional V-shape IPM machine in Toyota Prius 2010 [60]. Some key parameters of selected AIPM machines and IPM benchmark machine for Prius 2010 are given in Table II. The torque performance of these machines is calculated by using finite element (FE) analysis.

TABLE II
KEY DESIGN PARAMETERS OF MACHINES

Parameters	Unit	Values
Number of stator slots, N_s	-	48
Number of turns per slot, N_c	-	11
Stator outer radius, R_{sout}	mm	132
Stator slot height, h_s	mm	31
Stator tooth width, w_s	mm	7.3
Winding type	-	Single-layer short-pitch winding
Number of pole pairs, p	-	4
Air gap length, g	mm	0.82
Axial length, L_{st}	mm	50.8
Rotor inner radius, R_{rin}	mm	45
Rotor outer radius, R_{rout}	mm	80.22
Total PM volume, V_{mag}	mm^3	104460
Remanence of PMs, B_{res}	T	1.051
Coercivity of PMs, H_{ci}	MA/m	1.03

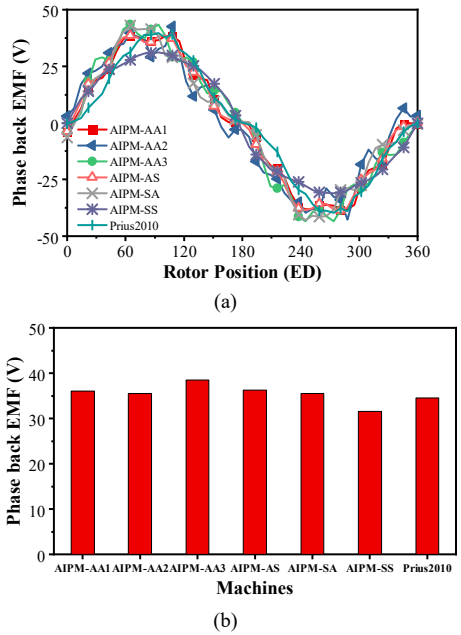

Fig. 18. Comparison of phase back EMFs. (a) Waveforms. (b) Amplitudes of the fundamental.

The phase back electromotive forces (EMFs) of AIPM machines and the Prius 2010 benchmark are compared in Fig. 18. The maximum synthetic, PM, and reluctance torque components of selected AIPM machines and IPM benchmark machine at 236A and 750 r/min by applying maximum torque per ampere method are extracted by using frozen permeability method [61] and are compared in Fig. 19. All AIPM machines show the increase of average torque with the same PM usage as the IPM machine. The maximum average torques of these machines at different currents are compared in Fig. 20, which reveals the increase of average torque in AIPM machines across the wide range of current, except for AIPM-SS that shows smaller torque at low current conditions, compared with the IPM benchmark machine. Thus, the torque enhancement of AIPM machines by utilizing MFS effect has been confirmed. More specifically, three selected AIPM machines with both asymmetric PMs and rotor geometry and the AIPM-AS machine with asymmetric hybrid pole structure show relatively higher average torque than other machines at 236A, but the maximum torque of AIPM-AS machine is smaller than those of three AIPM-AA machines when current is smaller than 200A. Three selected AIPM machines with both asymmetric PMs and rotor core, i.e. AIPM-AA1, AIPM-AA2, and AIPM-AA3, show similar maximum torque across the whole current range, although both the amplitudes of PM and reluctance torque in AIPM-AA3 machine with mixed radial and circumferential PMs are clearly higher than AIPM-AA1 and AIPM-AA2 machines with hybrid-layer PMs and outer flux barrier structure, respectively.

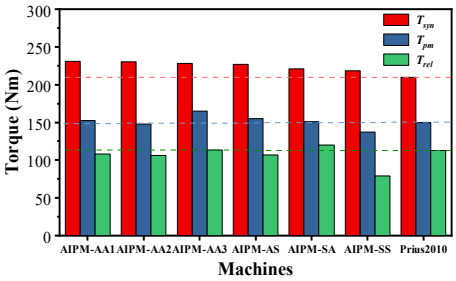

Fig. 19. Comparison of amplitudes of torque components

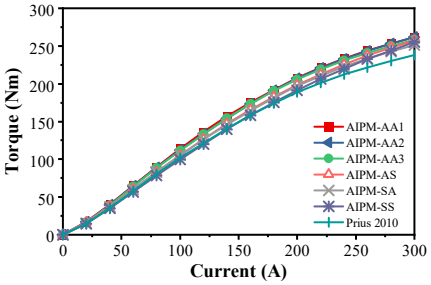

Fig. 20. Comparison of maximum average torque versus current.

B. Comparison between Inner and Outer Flux Barrier Designs and Experimental Validation

To illustrate the difference of maximum average torque in AIPM machine topologies with inner flux barrier [38]-[39] and outer flux barrier [56] designs, both topologies are employed in a 24-slot/4-pole AIPM machine with the same stator, rotor diameter, PM dimensions, and pole arc of PMs θ_{pm} (106 ED), as shown in Figs. 21 (a) and (b), respectively. The influence of flux barrier position with both inner and outer flux barrier designs on maximum torque at 10A, 1500 r/min and MTPA is shown in Fig. 21 (c). It reveals that the

AIPM machine with outer flux barrier structure can achieve higher maximum torque density than the counterpart with inner flux barrier design. The AIPM machine with outer flux barrier design has been prototyped and measured as shown in Fig. 22. The static torque performance between FE-predicted and measured results are compared in Fig. 23 for verification.

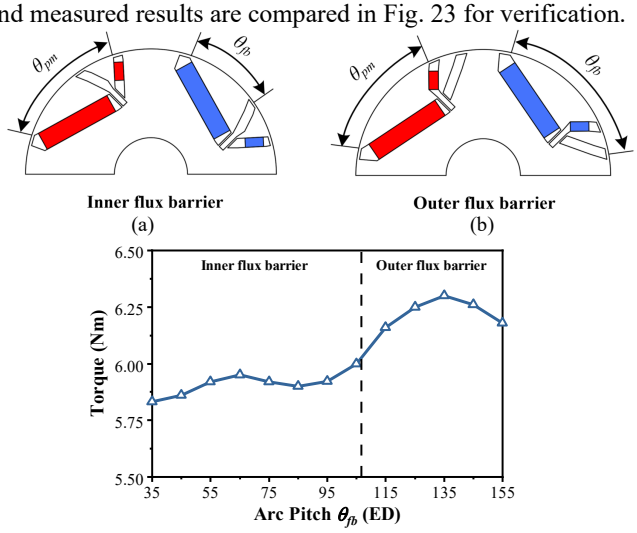

Fig. 21. Comparison between AIPM machines with asymmetric V-shape PMs. (a) Rotor with inner flux barrier [38]-[39]. (b) Rotor with outer flux barrier [56]. (c) Average torque versus flux barrier position at 10A, MTPA.

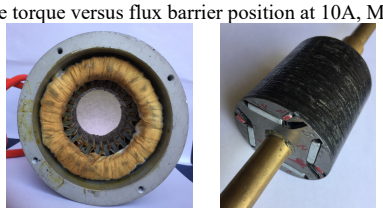

Fig. 22. Photos of the prototype [56]. (a) Stator. (b) Rotor.

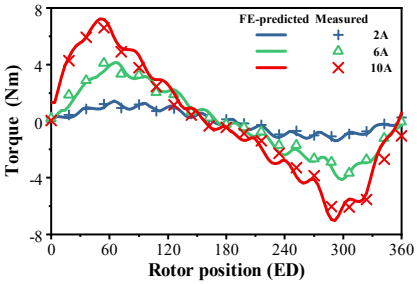

Fig. 23. Comparison of FE-predicted and measured static torque waveforms.

V. Conclusion

Based on the proposed categorization method, this paper has overviewed novel MFS techniques for torque enhancement in various asymmetric rotor pole IPM machine topologies. The relative merits and demerits of various AIPM rotor topologies have been analyzed, together with a comparison of torque capabilities of selected AIPM machines. It confirms that torque density can be enhanced by employing MFS effect and asymmetries in PM configuration and rotor core geometry. AIPM machines show competitive CPSR and flux weakening capability, and similar cross-coupling effect between *d*- and *q*-axes, compared with conventional IPM machines [56]. Thus, AIPM machines can be potential alternatives to conventional IPM topologies. However, many other issues, such as iron loss, efficiency, and mechanical and thermal characteristics [56], as well as noise and vibration, should also be considered in the design of AIPM machines.

References

[1] Z. Zhu and D. Howe, "Electrical machines and drives for electric, hybrid, and fuel cell vehicles," *Proc. IEEE*, vol. 95, no. 4, pp. 746-765, Apr. 2007.

[2] Z. S. Du and T. A. Lipo, "Cost-effective high torque density bi-magnet machines utilizing rare earth and ferrite permanent magnets," *IEEE Trans. Energy Convers.*, vol. 35, no. 3, pp. 1577-1584, Sept. 2020.

[3] D. G. Dorrell, M. Hsieh, M. Popescu, L. Evans, D. A. Staton, and V. Grout, "A review of the design issues and techniques for radial-flux brushless surface and internal rare-earth permanent-magnet motors," *IEEE Trans. Ind. Electron.*, vol. 58, no. 9, pp. 3741-3757, Sept. 2011.

[4] T. A. Lipo and W. Liu, "Comparison of AC motors to an ideal machine part I—conventional AC machines," *IEEE Trans. Ind. Appl.*, vol. 56, no. 2, pp. 1346-1355, Mar.-Apr. 2020.

[5] Z. Q. Zhu, W.Q. Chu, and Y. Guan, "Quantitative comparison of electromagnetic performance of electrical machines for HEVs/EVs," *CES Trans. on Electr. Mach. & Syst.*, vol. 1, no. 1, pp. 37-47, Jul. 2017.

[6] I. Boldea, L. N. Tutelea, L. Parsa, and D. Dorrell, "Automotive electric propulsion systems with reduced or no PMs: An overview," *IEEE Trans. Ind. Electron.*, vol. 61, no. 10, pp. 5696-5711, Jan. 2014.

[7] A. M. El-Refaie, J. P. Alexander, S. Galioto, P. B. Reddy, K. Huh, P. D. Bock, and X. Shen, "Advanced high-power-density interior permanent magnet motor for traction applications," *IEEE Trans. Ind. Appl.*, vol. 50, no. 5, pp. 3235-3248, Feb. 2014.

[8] H. Yang, H. Lin and Z. Q. Zhu, "Recent advances in variable flux memory machines for traction applications: a review," *CES Trans. on Electr. Mach. and Syst.*, vol. 2, no. 1, pp. 34-50, Mar. 2018.

[9] M. Villani, F. P. Collazzo, M. Tursini, G. Fabri, and L. Castellini, "PM brushless motor design for helicopter tail rotor," *2016 XXII Int. Conf. Electr. Mach. (ICEM)*, Lausanne, 2016, pp. 2669-2675.

[10] P. Arumugam, Z. Xu, A.L. Rocca, G. Vakil, M. Dickinson, E. Amankwah, T. Hamiti, S. Bozhko, C. Gerada, and S. J. Pickering., "High-speed solid rotor PM machines: concept and design," *IEEE Trans. Transp. Electrif.*, vol. 2, no. 3, pp. 391-400, Sept. 2016.

[11] B. Ruzojcic, D. Zarko and D. Ban, "Interior permanent-magnet motor for ship propulsion, design and testing," *2009 13th Eur. Conf. Power Electro. and Appl.*, Barcelona, 2009, pp. 1-10.

[12] Z. Zhang, J. Huang, Y. Jiang, W. Geng and Y. Xu, "Overview and analysis of PM starter/generator for aircraft electrical power systems," *CES Trans. on Electr. Mach. and Syst.*, vol. 1, no. 2, pp. 117-131, 2017.

[13] Y. Yang, S. M. Castano, R. Yang, M. Kasprzak, B. Bilgin, A. Sathyan, H. Dadkhah, and A. Emadi, "Design and comparison of interior permanent magnet motor topologies for traction applications," *IEEE Trans. on Transp. Electrif.*, vol. 3, no. 1, pp. 86-97, Oct. 2016.

[14] X. Liu, H. Chen, J. Zhao, and A. Belahcen, "Research on the performances and parameters of interior PMSM used for electric vehicles," *IEEE Trans. Ind. Electron.*, vol. 63, no. 6, pp. 3533-3545, Jun. 2016.

[15] Y. Hu, S. Zhu, C. Liu, and K. Wang, "Electromagnetic performance analysis of interior PM machines for electric vehicle applications," *IEEE Trans. Energy Convers.*, vol. 33, no. 1, pp. 199-208, Mar. 2018.

[16] S. Zhu, W. Chen, M. Xie, C. Liu, and K. Wang, "Electromagnetic performance comparison of multi-layered interior permanent magnet machines for EV traction applications," *IEEE Trans. Magn.*, vol. 54, no. 11, pp. 1-5, Nov. 2018.

[17] F. Momen, K. Rahman, and Y. Son, "Electrical propulsion system design of Chevrolet Bolt battery electric vehicle," *IEEE Trans. Ind. Appl.*, vol. 55, no. 1, pp. 376-384, Jan.-Feb. 2019.

[18] J. M. Seo, A. R. Ro, R. E. Kim, and J. Seo, "Hybrid analysis method considering the axial flux leakage in spoke-type permanent magnet machines," *IEEE Trans. Magn.*, vol. 56, no. 9, pp. 1-6, Sept. 2020.

[19] T. A. Huynh and M. F. Hsieh, "Comparative study of PM-assisted SynRM and IPMSM on constant power speed range for EV applications," *IEEE Trans. Magn.*, vol. 53, no. 11, pp. 1-6, May 2017.

[20] H. Cai, B. Guan, and L. Xu, "Low-cost ferrite PM-assisted synchronous reluctance machine for electric vehicles," *IEEE Trans. Ind. Electron.*, vol. 61, no. 10, pp. 5741-5748, Feb. 2014.

[21] P. Winzer and M. Doppelbauer, "Theoretical analysis of synchronous machines with displaced reluctance axis," *2014 Int. Conf. Electr. Mach. (ICEM)*, Berlin, 2014, pp. 641-647.

[22] W. Zhao, F. Zhao, T. A. Lipo, and B.I. Kwon, "Optimal design of a novel V-type interior permanent magnet motor with assisted barriers for the improvement of torque characteristics," *IEEE Trans. Magn.*, vol. 50, no. 11, pp. 1-4, Dec. 2014.

[23] H. Yang, Y. Li, H. Y. Lin, Z. Q. Zhu, S. Lyu, H. Wang, S. Fang, and Y. Huang, "Novel reluctance axis shifted machines with hybrid rotors," *2017 IEEE Energy Convers. Congr. Exposition (ECCE)*, Cincinnati, OH, USA, 2017, pp. 2362-2367.

[24] F. Xing, W. Zhao, and B.I. Kwon, "Design and optimisation of a novel asymmetric rotor structure for a PM-assisted synchronous reluctance machine," *IET Electr. Power Appl.*, vol. 13, no. 5, pp. 573-580, May 2018.

[25] Y. Xiao, Z. Q. Zhu, J. T. Chen, D. Wu, and L. M. Gong, "A novel asymmetric interior permanent magnet synchronous machine," *2020 Int. Conf. Electr. Mach. (ICEM)*, Gothenburg, 2020, pp. 26-32.

[26] D. F. Gosden, B. J. Chalmers, and L. Musaba, "Drive system design for an electric vehicle based on alternative motor types," in *1994 Fifth Int. Conf. Power Electron. Variable-Speed Drives*, 1994, pp. 710-715.

[27] B. J. Chalmers, L. Musaba, and D. F. Gosden, "Variable-frequency synchronous motor drives for electric vehicles," *IEEE Trans. Ind. Appl.*, vol. 32, no. 4, pp. 896-903, Jul.-Aug. 1996.

[28] D. F. Gosden and B. J. Chalmers, "Field weakening performance of a synchronous motor with two-part rotor," *1997 Eighth Int. Conf. Power Electron. Variable-Speed Drives*, 1997, pp. 244-247.

[29] B. J. Chalmers, R. Akmese, and L. Musaba, "Design and field-weakening performance of permanent-magnet/reluctance motor with two-part rotor," *IEE Proc.-Electr. Power Appl.*, vol. 145, no. 2, pp. 133-139, Mar. 1998.

[30] E. K. Beser, S. Camur, B. Arifoglu, and E. Beser, "Analysis and application of a hybrid motor structure convenient to modify the magnet and reluctance torques on the rotor," *J. Elec. Eng. &Tech.*, vol. 7, no. 3, pp. 349-357, Feb. 2012

[31] W. Zhao, F. Xing, X. Wang, T. A. Lipo, and B. Kwon, "Design and analysis of a novel PM-assisted synchronous reluctance machine with axially integrated magnets by the finite-element method," *IEEE Trans. Magn.,* vol. 53, no. 6, pp. 1-4, Jun. 2017.

[32] Y. Chen, J. Zhuang, T. Cai, Q. Wang, and W. Pu, "Design and analysis of a new less-rare-earth permanent magnet motor with axial hybrid rotors," *The 22nd Int. Conf. Electr. Mach. Syst. (ICEMS)*, 2019, pp. 1-4.

[33] W. Zhao, H. Shen, T. A. Lipo, and X. Wang, "A new hybrid permanent magnet synchronous reluctance machine with axially sandwiched magnets for performance improvement," *IEEE Trans. Energy Convers.*, vol. 33, no. 4, pp. 2018-2029, Dec. 2018.

[34] D. Bobba and B. Sarlioglu, "A unified model for field weakening operation of synchronous AC machines," *2020 IEEE Energy Convers. Congr. and Exposition (ECCE)*, Detroit, 2020, pp. 1418-1425.

[35] D. Bobba, T. A. Burress, J. Pries, and B. Sarlioglu, "Three-part hybrid rotor PM machine with variable magnetization state," *2017 IEEE Energy Convers. Congr. and Exposition (ECCE)*, Cincinnati, OH, 2017, pp. 1240-1246.

[36] S. Hayslett and E. Strangas, "Design and analysis of aligned axis interior permanent magnet machines considering saturation," *2019 IEEE Int. Electr. Mach. & Drives Conf. (IEMDC)*, San Diego, CA, USA, 2019, pp. 686-692.

[37] Y. Fan, C. Tan, S. Chen, and M. Cheng, "Design and analysis of a new interior PM motor for EVs," *The 8th Int. Power Electron. Motion Control Conf. (IPEMC-ECCE Asia)*, Hefei, 2016, pp. 1357-1361.

[38] T. Takahashi, Y. Miyama, M. Nakano, and K. Yamane, "Permanent magnet rotating electric machine," Japan and PCT Patent Appl. WO 2019/064801 A1, Apr. 4, 2019.

[39] K. Yamazaki and R. Kondo, "Reduction of cross magnetization in interior permanent magnet synchronous motors with V-shape magnet configurations by optimizing rotor slits," *2019 IEEE Energy Convers. Congr. Exposition (ECCE)*, Baltimore, MD, USA, 2019, pp. 4873-4879.

[40] Y. Xiao, Z. Q. Zhu, J. T. Chen, D. Wu, and L. M. Gong, "A novel V-shape interior permanent magnet synchronous machine with asymmetric spoke-type flux barrier," *2020 Int. Conf. Electr. Mach. (ICEM)*, Gothenburg, 2020, pp. 382-388.

[41] Y. Xiao, Z. Q. Zhu, J. T. Chen, D. Wu, and L. M. Gong, "A novel spoke-type asymmetric rotor interior PM machine," 2020 *IEEE Energy Convers. Congr. Exposition (ECCE)*, Detroit, MI, USA, 2020, pp. 4050-4057.

[42] Y. Jung, M. Park, and M. Lim, "Asymmetric rotor design of IPMSM for vibration reduction under certain load condition," *IEEE Trans. Energy Convers.*, vol. 35, no. 2, pp. 928-937, Jun. 2020.

[43] J. Y. Alsawalhi and S. D. Sudhoff, "Effects of positioning of permanent magnet axis relative to reluctance axis in permanent magnet synchronous machines," *2015 IEEE Power and Energy Conf. at Illinois* (PECI), Champaign, IL, 2015, pp. 1-8.

[44] J. Y. Alsawalhi and S. D. Sudhoff, "Design optimization of asymmetric salient permanent magnet synchronous machines," *IEEE Trans. Energy Convers.*, vol. 31, no. 4, pp. 1315-1324, Dec. 2016.

[45] A. Kasha, R. Lin, S. Sudhoff, J. Chalfant, and J. Alsawalhi, "A comparison of permanent magnet machine topologies for marine propulsion applications," *2017 IEEE Electr. Ship Technol. Symp. (ESTS)*, Arlington, VA, 2017, pp. 437-444.

[46] G. Liu, G. Xu, W. Zhao, X. Du, and Q. Chen, "Improvement of torque capability of permanent-magnet motor by using hybrid rotor configuration," *IEEE Trans. Energy Convers.*, vol. 32, no. 3, pp. 953-962, Sept. 2017.

[47] G. Xu, G. Liu, W. Zhao, Q. Chen, and X. Du, "Principle of torque-angle approaching in a hybrid rotor permanent-magnet motor," *IEEE Trans. Ind. Electron.*, vol. 66, no. 4, pp. 2580-2591, Apr. 2019.

[48] Y. Li, H. Yang, H. Lin, S. Fang, and W. J. E. Wang, "A novel magnet-axis-shifted hybrid permanent magnet machine for electric vehicle applications," *Energies*, vol. 12, no. 4, pp. 641-653, 2019.

[49] H. Yang, W. Wang, H. Lin, Z. Q. Zhu, S. Lyu, and S. Niu, "A novel hybrid-pole interior PM machine with magnet-axis-shifting effect," *2019 IEEE Int. Electr. Mach. & Drives Conf. (IEMDC)*, San Diego, CA, USA, 2019, pp. 273-279.

[50] Z. Ji, H. Li, Z. Chen, T. Yu, L. Liu, and M. Ma, "Design and optimization of permanent magnet assisted synchronous reluctance motor for better torque performance," *2019 22nd Int. Conf. Electr. Mach. and Syst. (ICEMS)*, Harbin, China, 2019, pp. 1-4.

[51] W. Zhao, D. Chen, T. A. Lipo, and B. Kwon, "Performance improvement of ferrite-assisted synchronous reluctance machines using asymmetrical rotor configurations," *IEEE Trans. Magn.*, vol. 51, no. 11, pp. 1-4, Nov. 2015.

[52] M. Ibrahim and P. Pillay, "Aligning the reluctance and magnet torque in permanent magnet synchronous motors for improved performance," *2018 IEEE Energy Convers. Congr. Exposition (ECCE)*, Portland, OR, 2018, pp. 2286-2291.

[53] R. Thike and P. Pillay, "Mathematical model of an interior PMSM with aligned magnet and reluctance torques," *IEEE Trans. Transp. Electrif.*, vol. 6, no. 2, pp. 647-658, Jun. 2020.

[54] W. Zhao, T. A. Lipo, and B. Kwon, "Optimal design of a novel asymmetrical rotor structure to obtain torque and efficiency improvement in surface inset PM motors," *IEEE Trans. Magn.*, vol. 51, no. 3, pp. 1-4, Mar. 2015.

[55] W. Ren, Q. Xu, and Q. Li, "Asymmetrical V-shape rotor configuration of an interior PM machine for improving torque characteristics," *IEEE Trans. Magn.*, vol. 51, no. 11, pp. 1-4, Nov. 2015.

[56] Y. Xiao, Z. Q. Zhu, S. S. Wang, G. W. Jewell, J. T. Chen, D. Wu, and L. M. Gong, "A novel asymmetric interior permanent magnet machine for electric vehicles," *IEEE Trans. Energy Convers.*, in press.

[57] X. Zeng, L. Quan, X. Zhu, L. Xu, and F. Liu, "Investigation of an asymmetrical rotor hybrid permanent magnet motor for approaching maximum output torque," *IEEE Trans. Appl. Supercond.*, vol. 29, no. 2, pp. 1-4, Mar. 2019.

[58] Y. Xiao, Z. Q. Zhu, J. T. Chen, D. Wu, and L. M. Gong, "A novel asymmetric interior permanent magnet synchronous machine," *2020 Int. Conf. Electr. Mach. (ICEM)*, Gothenburg, 2020, pp. 26-32.

[59] P. Winzer and M. Doppelbauer, "Comparison of synchronous machine designs with displaced reluctance axis considering losses and iron saturation," *2015 IEEE Int. Electr. Mach. & Drives Conf. (IEMDC)*, Coeur d'Alene, ID, 2015, pp. 1801-1807.

[60] T. A. Burress, S. L. Campbell, C. L. Coomer, C. W. Ayers, A. A. Wereszczak, J. P. Cunningham, L. D. Marlino, L. E. Seiber, and H. T. Lin, "Evaluation of the 2010 Toyota Prius hybrid synergy drive system," Oak Ridge Nat. Lab., Oak Ridge, TN, USA, Rep. ORNL/TM2010/253, 2010.

[61] Z.Q. Zhu and W.Q. Chu, "Advanced frozen permeability technique and applications in developing high performance electrical machines," *Trans. of China Electrotech. Soc.*, vol.31, no.20, pp.13-29, Oct. 2016.